NANO LETTERS

pubs.acs.org/NanoLett

Mini-Review

Engineering Two-Dimensional Magnetic Heterostructures: A Theoretical Perspective

Jinbo Pan, Yan-Fang Zhang, Yu-Yang Zhang, and Shixuan Du*

Cite This: https://doi.org/10.1021/acs.nanolett.4c04251

Read Online

ACCESS | Metrics & More | Article Recommendations

ABSTRACT: Two-dimensional (2D) magnetic materials have attracted great attention due to their promise for applications in future high-speed, low-energy quantum computing and memory devices. By integrating 2D magnetic materials with other magnetic or nonmagnetic materials to form heterostructures, the synergistic effects of interlayer orbital hybridization, spin−orbit coupling, and symmetry breaking can surpass the performance of single-layer materials and lead to novel physical phenomena. This review provides a comprehensive theoretical analysis of engineering 2D magnetic heterostructures, emphasizing the fundamental physics of interlayer interactions and the resulting enhancements and novel properties. It reviews the mechanisms and progress in tuning the magnetic ordering, enhancing the Curie temperature (T_c) and modulating properties such as topological magnetic structures, spin polarization, electronic band topology, valley polarization, and magnetoelectric coupling through the construction of 2D magnetic heterostructures. Additionally, this review discusses the current challenges faced by 2D magnetic heterostructures, aiming to guide the future design of higher-performance magnetic heterostructures.

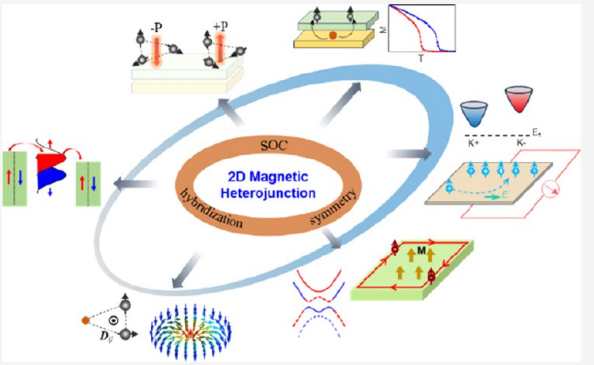

KEYWORDS: *2D Magnetic Heterostructures, Spintronics, Quantum Anomalous Hall Effect, Skyrmions, Multiferroics*

In 1966, Mermin and Wagner, through rigorous theoretical derivation, proposed that long-range magnetic order cannot exist in isotropic Heisenberg low-dimensional systems.[1] This led to a long-standing belief that the same principle could be applied universally to all low-dimensional magnetic systems. In 2017, the discovery of long-range magnetic order in 2D CrI_3[2] and $CrGeTe_3$[3] marked a significant milestone in condensed matter physics and materials science, stimulating intense research interest in 2D magnetic materials. The 2D magnetic materials, with their atomic-scale thickness and pristine, dangling-bond-free surfaces, offer a versatile platform for exploring magnetic properties at the atomic scale level. They also enable precise control of magnetism through external fields and interfacial engineering, as well as the study of coupling effects among different order parameters and novel tuning mechanisms.[4,5]

As one of the interface systems, a 2D magnetic heterojunction can be created by stacking 2D magnetic material with other 2D materials, resulting in a complex system in which interlayer interactions can lead to unique and emergent properties. For instance, the interfacial interaction can enhance the T_c, leading to more robust magnetic ordering at high temperatures.[6] A high T_c is crucial for practical applications in spintronics and magnetic memory devices. Moreover, 2D magnetic heterojunctions provide a fertile ground for the emergence of exotic magnetic textures such as skyrmions,[7] which are topologically protected spin configurations with potential applications in high-density data storage and spintronic devices. The interface-induced interactions in 2D magnetic heterojunctions play a crucial role in stabilizing skyrmions, making it possible to stabilize and manipulate skyrmions under conditions that may not be achieved in their bulk counterparts or single-layer 2D systems. In the field of spintronics, 2D magnetic heterojunctions offer promising prospects by enabling efficient spin injection, manipulation, and detection at the nanoscale.[8] The interface interactions can lead to spin filtering effects and other phenomena that are pivotal for developing next-generation spintronic devices.[9] Furthermore, the interplay between magnetism and topology in 2D magnetic heterojunctions can give rise to magnetic topological properties, such as the quantum anomalous Hall effect.[10] These properties are of significant interest for both fundamental physics and potential applications in low-dissipation electronic devices.

Received: August 30, 2024
Revised: November 14, 2024
Accepted: November 14, 2024

Beyond magnetism, 2D magnetic heterojunctions exhibit multifunctional properties such as multiferroicity, where magnetic and ferroelectric (FE) orders coexist,[11] and superconductivity, which can be tuned by interlayer coupling.[12] These multifunctionalities open up new possibilities for designing hybrid devices that leverage multiple properties simultaneously. Additionally, the optical properties of 2D magnetic heterojunctions are significantly influenced by interlayer interactions, leading to phenomena such as enhanced magneto-optical effects,[13] tunable photoluminescence,[14] and novel excitonic behaviors.[15] These optical properties are crucial for the development of advanced optoelectronic and photonic devices.

Recently, several review articles related to 2D magnetic heterojunctions have been published.[4,5,16] For example, Li et al. summarized different theoretical models to describe magnetic ordering, and methods to tune magnetism in 2D magnetic materials in 2021.[5] Choi et al. reviewed the intuitive origin of the magnetic proximity effect, methods to determine interfacial magnetism, and observing proximity-related phenomena in heterostructures in 2022.[4] Jiang et al. focused on the properties and potential applications of 2D magnetic Janus monolayers and their heterostructures. From a theoretical point of view, they reviewed the theoretical methodologies for describing magnetic properties, the effects of built-in polarization fields, and demonstrated tunable T_c and spin textures in the heterostructures with different stacking modes.[16] Despite these valuable contributions, a review that specifically targets the complex mechanisms of interlayer interactions and their profound influence on the emergent properties of 2D magnetic heterojunctions remains absent. Moreover, with the field advancing rapidly and discoveries emerging continuously, an updated review is essential to capture the latest breakthroughs.

Here, we aim to provide a theoretical review of 2D magnetic heterojunctions, focusing on the mechanisms of interlayer interactions and the enhanced and emergent properties induced by these interactions. By understanding the fundamental principles and mechanisms that govern 2D magnetic heterojunctions, we can better utilize the unique properties of 2D magnetic heterojunctions for various technological applications. This Mini-Review summarizes current challenges and guides future research directions, making it a valuable resource for both experienced researchers and newcomers to the field. It holds a significant reference value in spintronics, optoelectronics, quantum computing, and other related areas.

Ignoring higher-order magnetic interactions and magnetic exchange anisotropy, magnetic interactions Hamiltonian can be expressed as[17]

$$\hat{H} = \sum_{i<j} J_{ij}\hat{S}_i \bullet \hat{S}_j + \sum_{i<j} \vec{D}_{ij} \bullet (\hat{S}_i \times \hat{S}_j) + \sum_i A_i S_{iz}^2 \quad (1)$$

where $\hat{S}_i$ and $\hat{S}_j$ represent spins at different sites, and J_{ij}, $\vec{D}_{ij}$, A_i are magnetic exchange interaction, Dzyaloshinskii-Moriya interaction (DMI), and magnetocrystalline anisotropy energy (MAE) parameters, respectively. The exchange interaction arises from the interplay between the Coulombic and kinetic exchanges. The overlap of wave functions determines the former, while the latter is associated with various mechanisms, including direct exchange, superexchange, supersuper exchange, and double exchange.[18] For the 2D magnetic materials with large distances between neighboring magnetic atoms, the direct wave function overlap and direct exchange can be ignored, while the indirect exchange interaction dominates. A schematic diagram of the exchange interaction and the phenomenological mechanism are shown in Figure 1a,b. The

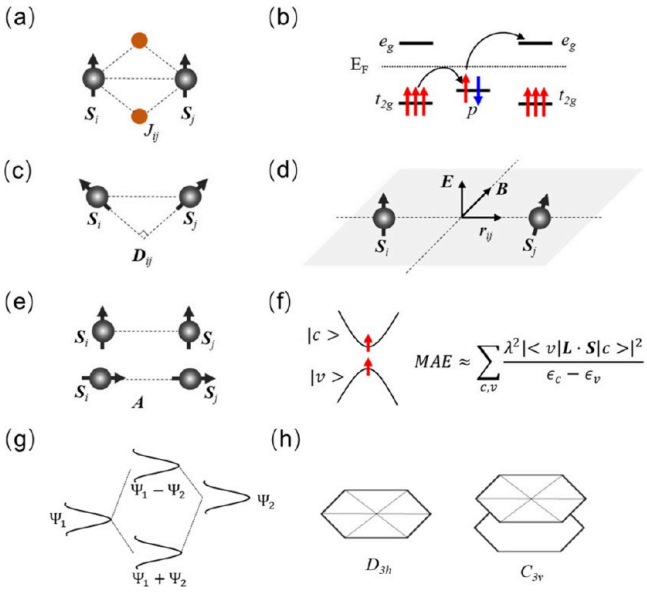

Figure 1. Schematics of the magnetic interactions and interlayer interaction. (a) and (b) FM superexchange interaction via intermediate atoms. Arrows represent the direction of spins. (c) and (d) Schematic of DMI and origin of DMI. $\boldsymbol{r}_{ij}$ is the unit vector points from site i to j. (e) and (f) Schematic and origin of magnetic crystalline anisotropy. (g) Schematic illustration of energy level splitting owing to the interlayer hybridization; Ψ_1 and Ψ_2 are the wave functions of the individual layers. (h) Schematic of symmetry variations induced by interlayer stacking.

strength of the exchange interaction between the two spin sites is proportional to the hopping integral t for the ferromagnetic (FM) arrangement, but *to* t^2/U for the antiferromagnetic (AFM) arrangement.[17]

DMI originates from spin−orbit coupling (SOC) in the system absent of inversion symmetry and leads to the noncolinear spin arrangement of spin texture (Figure 1c). The mechanism of DMI can be described as follows (see Figure 1d).[19] The breaking of spatial inversion symmetry results in an atomic electric field ($\boldsymbol{E}$). During the hopping process of electrons from the $\boldsymbol{S}_i$ to the $\boldsymbol{S}_j$ site, the movement of the electric field results in the generation of an additional magnetic field ($\boldsymbol{B}$) along the direction of $\boldsymbol{E} \times \boldsymbol{r}_{ij}$. Influenced by the magnetic field, the electron spin acquires an additional exchange interaction when it arrives at the j site: $\boldsymbol{S}_j \cdot (\boldsymbol{B} \times \boldsymbol{S}_i) = \boldsymbol{B} \cdot (\boldsymbol{S}_i \times \boldsymbol{S}_j)$, i.e., the emergence of DMI.

Magnetic crystalline anisotropy is also a consequence of spin−orbit coupling and can be evaluated by the perturbation theory. Due to the typically quenched orbital momentum of magnetic materials, the second-order perturbation mainly contributes to the MAE as follows:[20]

https://doi.org/10.1021/acs.nanolett.4c04251
Nano Lett. XXXX, XXX, XXX−XXX

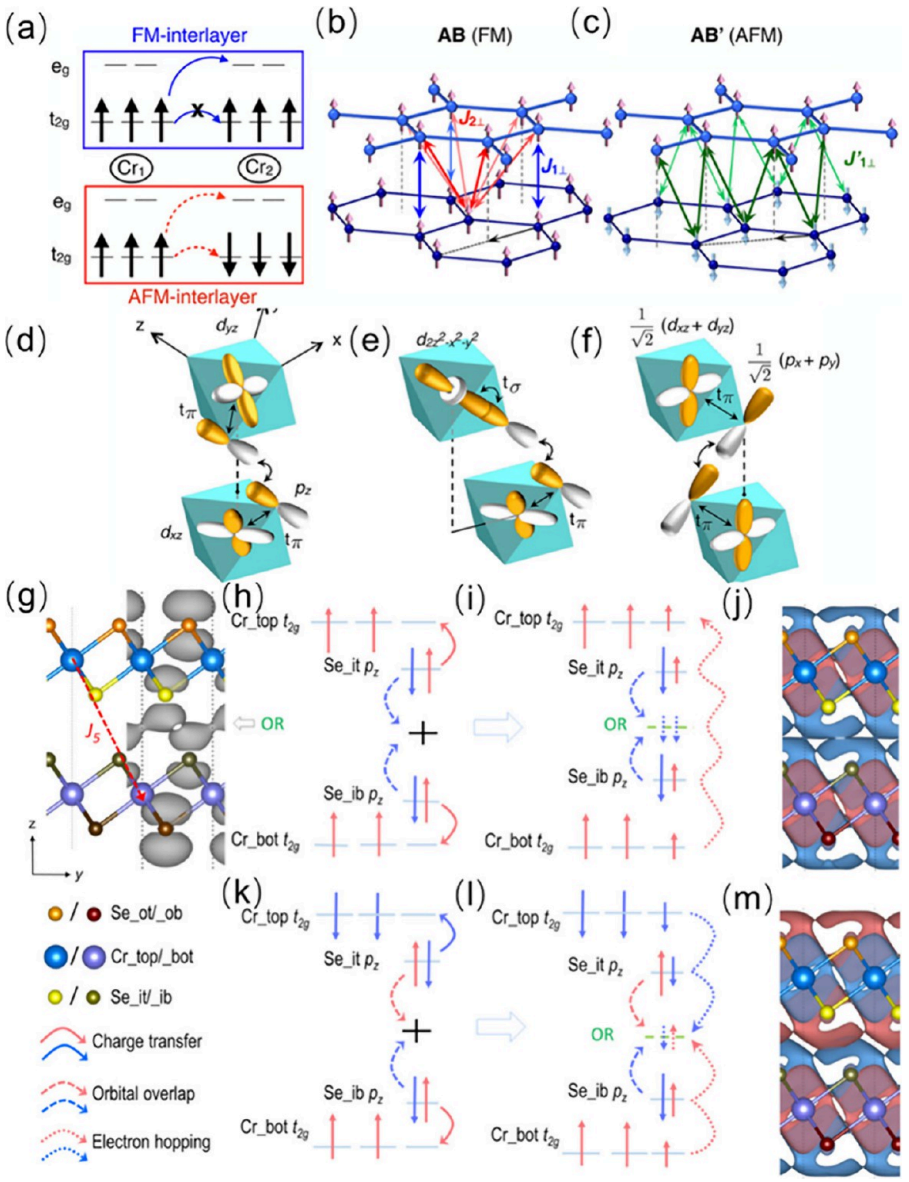

Figure 2. Magnetic ordering transition modulated by interlayer magnetic coupling, i.e. through interlayer sliding[23] (a–f) Copyright 2018, American Chemical Society, and vertical strain.[24] (g–m) Copyright 2020, American Physical Society. (a) Schematic of the orbital dependent interlayer supersuper exchange (SSE) interactions of bilayer CrI_3. (b) Interlayer nearest-neighbor ($J_{1\perp}$, in blue) interaction and the second-neighbor ($J_{2\perp}$, in red) interaction in AB-stacking and (c) the nearest-neighbor ($J'_{1\perp}$, in green) interaction in AB′-stacking. Schematics for (d) the AFM SSE $J_{1\perp}$ involving half-filled t_{2g} orbitals, (e) the FM SSE $J_{2\perp}$ between half-filled t_{2g} orbital and empty e_g orbital, and (f) the AFM SSE $J'_{1\perp}$ between half-filled t_{2g} orbitals. (g) Side view of bilayer $CrSe_2$ indicative of spin-exchange coupling J5 and mapped with the wave function norms of the Se $4p_z$ bonding state where an overlapped region (OR) was identified. Panels (h) and (k) are schematics of the interlayer charge transfer and wave function overlaps. Panels (i) and (l) illustrate spin-exchange mechanisms of the interlayer FM (h, i) and AFM (k, l) configurations, respectively. Spin-up and -down electrons are represented by red straight-up and blue straight-down arrows, the length of which qualitatively represents the amount of spin polarized electrons. Red (spin-up) and blue (spin-down) curved arrows indicate the charge transfer (solid), wave function overlap (dashed), and electron hopping (dotted), respectively. Spin densities of the both configurations were plotted in (j) and (m), respectively, with an isosurface value of 0.0004 e/Bohr^3. Red and blue contours denote spin-up and -down, respectively.

$$\mathrm{MAE} = \lambda^2 \sum_{v,c,\sigma} (|\langle v, \sigma|L_z|c, \sigma <>\rangle|^2 - |\langle v, \sigma|L_x|c, \sigma <>\rangle|^2) / (\epsilon_{c,\sigma} - \epsilon_{v,\sigma}) + \lambda^2 \sum_{v,c,\sigma\neq\sigma'} (|\langle v, \sigma|L_x|c, \sigma' <>\rangle|^2 - |\langle v, \sigma|L_z|c, \sigma' <>\rangle|^2) / (\epsilon_{c,\sigma'} - \epsilon_{v,\sigma}) \quad (2)$$

where the first and second summations correspond to the spin conserving $|\Delta s_z| = 0$ and spin-flipping $|\Delta s_z| = 1$ transitions, and $|v,\sigma>$ and $|v,\sigma>$ are valence and conduction band states with spin σ, respectively, whose energy eigenvalues are $\epsilon_{c,\sigma}$ and $\epsilon_{v,\sigma}$. The angular momentum matrix elements of L_z and L_x correspond to transitions with $|\Delta m_z| = 0$ and $|\Delta m_z| = 1$ for d orbitals, respectively.

Constructing and regulating the properties of magnetic heterostructures involve several key aspects: enhancing the intrinsic properties of materials, generating new properties

https://doi.org/10.1021/acs.nanolett.4c04251
Nano Lett. XXXX, XXX, XXX−XXX

absent in the parent materials, and enabling reversible control among different properties. These objectives are primarily achieved through modulation of interlayer orbital hybridization and symmetry breaking, as shown in Figure 1g,h. The interlayer hybridization can be best described as covalent-like quasi-bonding (CLQB).[21] When dispersion forces lead to overlap between nonbonding frontier orbitals in adjacent layers, it results in electronic hybridization at van der Waals (vdW) gaps. This hybridization forms interfacial bonding and antibonding states, leading to interfacial charge redistribution similar to that observed in covalent bonds. However, a key distinction lies in that the numbers of electrons occupying the bonding and antibonding states remain equal after hybridization, preventing appreciable energy lowering, unlike true covalent bonds. The orbital hybridization and symmetry breaking are interdependent and influence each other. For example, symmetry breaking in the geometric structure often requires interlayer orbital hybridization to alter the electronic structure. Changes in the symmetry are usually accompanied by changes in interlayer orbital hybridization. In 2D heterostructures, delocalized out-of-plane orbitals such as d_{z^2} and p_z orbitals lead to stronger interlayer interactions. For 2D materials with similar structures and orbital compositions, the material with heavier elements at the interface generally exhibits stronger interlayer hybridization and SOC effect.

It is obvious that in 2D magnetic heterostructures the interlayer interactions lead to changes in the mediating orbitals of the superexchange coupling among magnetic atoms, thereby affecting the strength of magnetic exchange coupling. Additionally, orbital hybridization can influence the wave functions of the conduction band (CB) and valence band (VB) in the material system as well as their eigenvalues, which in turn affects the magnetic anisotropy. From a symmetry perspective, hetero stacking often results in reduced symmetry, as shown in Figure 1h. For instance, magnetic materials with a central inversion symmetry do not exhibit DMI. However, interfaces can break the central inversion symmetry, leading to the emergence of interface-induced DMI. For more details on the existence of DMI under different symmetries and the direction of DMI, one can refer to Moriya's rule.[22]

Interlayer interactions within van der Waals (vdW) gaps were previously considered to be quite weak, but recent studies have revealed that they can be strong enough in altering electronic structures and magnetic properties.[23,24] For example, Sivadas et al. reported that one can tune the interlayer exchange interaction between antiferromagnetic and ferromagnetic by changing the interlayer stacking order.[23] Wang et al. revealed that the tuning interlayer distance is another strategy to achieve the interlayer magnetic ordering transition.[24] The two different mechanisms are illustrated in Figure 2.

For bilayer CrI_3, the Cr atoms in CrI_3 are in a d^3 electronic configuration, and the top of the valence band and bottom of conduction band are made up of a combination of three t_{2g} orbitals, and two e_g orbitals, respectively. Figure 2a shows a schematic of the different exchange interactions between Cr atoms in different layers under the FM (blue) and AFM (red) alignment. Hopping of the form t_{2g}− t_{2g} is prohibited for FM alignment, whereas this is allowed for AFM alignment. Therefore, t_{2g}-t_{2g} hybridization leads to AFM, and hopping of the form t_{2g}−e_g leads to an exchange coupling that is predominantly FM. All these interlayer Cr−Cr exchange interactions are mediated by the hybridization between the I_p orbitals, i.e., supersuperexchange interaction (SSE). Under AB stacking (Figure 2b), the interlayer nearest-neighbors $J_{1\perp}$, and second neighbors $J_{2\perp}$ dominate the interlayer Cr−Cr interaction. The $J_{1\perp}$ is dominated by virtual t_{2g}-t_{2g} hoping, which induces an AFM coupling (Figure 2d). While the $J_{2\perp}$ is dominated by virtual t_{2g}-e_g hoping, resulting in an FM coupling (Figure 2e). There are one $J_{1\perp}$ bond and 16 $J_{2\perp}$ bonds per unit cell, making AB-stacking bilayer CrI_3 FM, while under AB' stacking (Figure 2c), there is only one type of interlayer Cr−Cr SSE interaction $J'_{1\perp}$ through virtual t_{2g}-t_{2g} hoping, leading to AFM alignment of bilayer CrI_3.

For bilayer $CrSe_2$, the magnetic ordering transition was found to be determined by a competition between Pauli repulsion at the interface region and kinetic-energy gain across the entire bilayer. In the $CrSe_2$ bilayer, two interfacial Se $4p_z$ orbitals overlap and hybridize into one bonding state (Figure 2g) and one antibonding state at the overlapped region (OR), which is an area accumulating shared charge from the interfacial Se atoms. In the interlayer FM configuration (Figure 2g−j), interfacial Se p_z orbitals strongly overlap, leading to charge transfer from the spin up channel of p_z orbitals to Cr t_{2g} orbitals, and spin down orbitals predominate at the OR (Figure 2h−j). Therefore, the interlayer spin-exchange coupling is depicted in Figure 2i. The spin-up electrons of Cr_bot t_{2g} could hop into the Se_ib $4p_z$ orbital, and then reach the OR, Se p_z orbital, and Cr_top t_{2g}. This substantially lowers the kinetic energy of spin-up electrons across the bilayer. However, the OR are effectively filled with two spin down fractional electrons, giving rise to an appreciable Pauli repulsive interaction. On the other hand, under AFM stacking (Figure 2k−m), the OR is composed of both spin components, and the Pauli repulsion is largely eliminated. However, such a configuration shortens the range that a spin-polarized electron can move across the bilayer, thus lifting up the kinetic energy. Therefore, competition between interlayer hopping and Pauli repulsion at the OR determines the interlayer magnetism. At a shorter interlayer distance, Pauli repulsion at the OR dominates and thus favors interlayer AFM. For a longer distance, kinetic-energy gain of polarized electrons across the bilayer balances the Pauli repulsion, and the bilayer thus prefers an interlayer FM state.

Room temperature magnetism in 2D materials is crucial for practical applications in spintronics and data storage, ensuring stable magnetic properties under typical operating conditions. Although numerous 2D magnetic materials have been discovered, only a few have a T_c above room temperature.[6,25] To overcome this challenge, engineering the magnetism of 2D materials through the proximity effect is a promising strategy.

Recently, Wang et al. reported a wafer-scale van der Waals (vdW) ferromagnet, Fe_4GeTe_2, with a T_c far above room temperature.[6] The vdW Fe_4GeTe_2 layers with different thicknesses were fabricated on a sapphire substrate. They observed an increase in T_c as the number of layers decreased. For 4 nm thick Fe_4GeTe_2, the magnetic order persists up to approximately 530 K, while T_c drops to around 270 K at a thickness of 16 nm. This behavior contrasts with traditional vdW ferromagnets, which typically experience a sharp decrease in T_c as the thickness decreases. The finding suggests the important role of interface modulation in the magnetism of Fe_4GeTe_2, with the bottom few layers most affected by the interface, resulting in the highest T_c. To quantify the interface contribution to the T_c enhancement, they theoretically calculated the magnetic interaction parameters and used the

https://doi.org/10.1021/acs.nanolett.4c04251
Nano Lett. XXXX, XXX, XXX−XXX

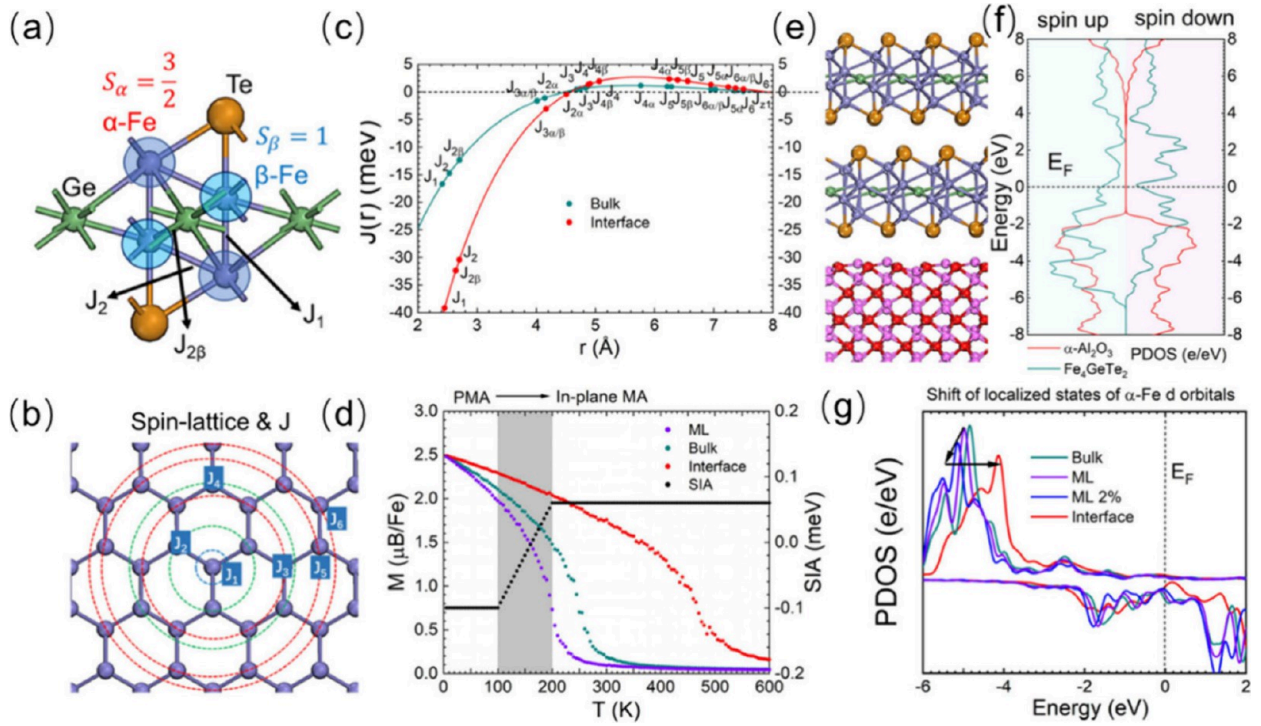

Figure 3. Interfacial interaction enhanced T_c of Fe_4GeTe_2.[6] Copyright 2023, Springer Nature. (a) Atomic structure of the unit cell of Fe_4GeTe_2. Two kinds of Fe with different symmetric positions and spins are marked as α-Fe and β-Fe. The most important three exchange interactions are marked as J_1, J_2, and $J_{2\beta}$. (b) Top view of the spin−lattice of Fe_4GeTe_2 and marked exchange interactions, only Fe atoms are shown. (c) J-r dispersion of bulk and interface-modulated Fe_4GeTe_2 obeying the RKKY rule. (d) Average magnetization per Fe versus temperature for the ML, bulk, and interface modulated Fe_4GeTe_2. The single-ion anisotropy energy (SIA) is marked in black. (e). Atomic structure of 2-layers Fe_4GeTe_2 onto the sapphire substrate. (f) PDOS of the Fe_4GeTe_2 and the substrate. (g) PDOS of the d orbitals of the α-Fe in bulk, ML with 2% strain and interface modulated Fe_4GeTe_2.

Monte Carlo (MC) method to simulate the T_c of pristine Fe_4GeTe_2 with different layers and bilayer Fe_4GeTe_2 on a sapphire substrate.

Due to the itinerant magnetism of Fe_4GeTe_2 and local magnetic moments of Fe, the exchange interactions can be described by the classic Heisenberg model with Ruderman−Kittle−Kasuya−Yosida (RKKY) exchange, which can be written as

$$H = \sum_{i<j} S_i^\alpha [J_{ij}]_{\alpha\beta} S_j^\beta + \sum_i A(S_i^z)^2 \tag{3}$$

where S_i^α is the spin operator on site i, and α, β can be x, y, z. The term $[J_{ij}]_{\alpha\beta}$ describes the Heisenberg exchange interactions between the spins on sites i and j. According to the mean-field theory, T_c is proportional to the overall exchange interaction as well as $S(S + 1)$, where S is the average onsite spin on Fe. Neglecting the nonisotropic exchanges, the Heisenberg exchange then degenerates into a scalar. The exchange interactions follow the RKKY rule:[26]

$$J(r) = -J^2 \times \frac{\sin(2k_F r) - 2k_F r \cos(2k_F r)}{(k_F r)^4} \tag{4}$$

where r is the distance between the two spin sites and k_F is the Fermi momentum of the itinerant electrons.

Figure 3a shows the primitive cell structure of the monolayer Fe_4GeTe_2, containing a dumbbell shape of four Fe atoms. There are three nearest-neighbor exchange interactions, called J_1, J_2, and $J_{2\beta}$, at a spatial distance of ∼2.5 Å. The other exchange interactions with Fe−Fe distances of >4 Å (Figure 3b) are less important according to the RKKY rule (Figure 3c). The nearest-neighbor exchange interaction of bulk Fe_4GeTe_2 is around 15 meV (Figure 3c), resulting in the estimated T_c's of bulk Fe_4GeTe_2 and monolayer Fe_4GeTe_2 both under 300 K. Monolayer Fe_4GeTe_2 possesses a lower T_c than its bulk counterpart (Figure 3d). Upon considering the Fe_4GeTe_2-sapphire interface, the nearest-neighbor exchange interaction of magnetic atoms reaches around 40 meV (Figure 3c), with the estimated T_c approaching around 500 K (Figure 3d). The interface induced increase of exchange interaction can be explained by the Anderson model, in which J is related to the distance between the Fermi level (E_F) and the localized states that contribute to the formation of magnetic moments (E_d), as well as the Hubbard U, which denotes the onsite Coulomb repulsion:[27]

$$J \approx -\frac{1}{E_F - E_d} + \frac{1}{E_F - E_d - U} \tag{5}$$

As shown in Figure 3e−f, E_F lies near the valence edge of Al_2O_3, and the spin-down bands of the metal inside the gap are mostly unoccupied, while those of spin-up are occupied. Figure 3g compares the projected density of states (PDOS) of the d orbitals of the α-Fe in bulk, monolayer, monolayer with strain, and interface structure. The thickness and 2% strain do not dramatically change the PDOS of the d orbitals, while the integration with the sapphire induces a right shift of unpaired Fe d electrons, which will move the E_d toward the E_F, and is the key factor leading to the enhancement of J.

Similar to T_c, the equilibrium magnetic structure is directly influenced by magnetic interactions. Among various magnetic

https://doi.org/10.1021/acs.nanolett.4c04251
Nano Lett. XXXX, XXX, XXX−XXX

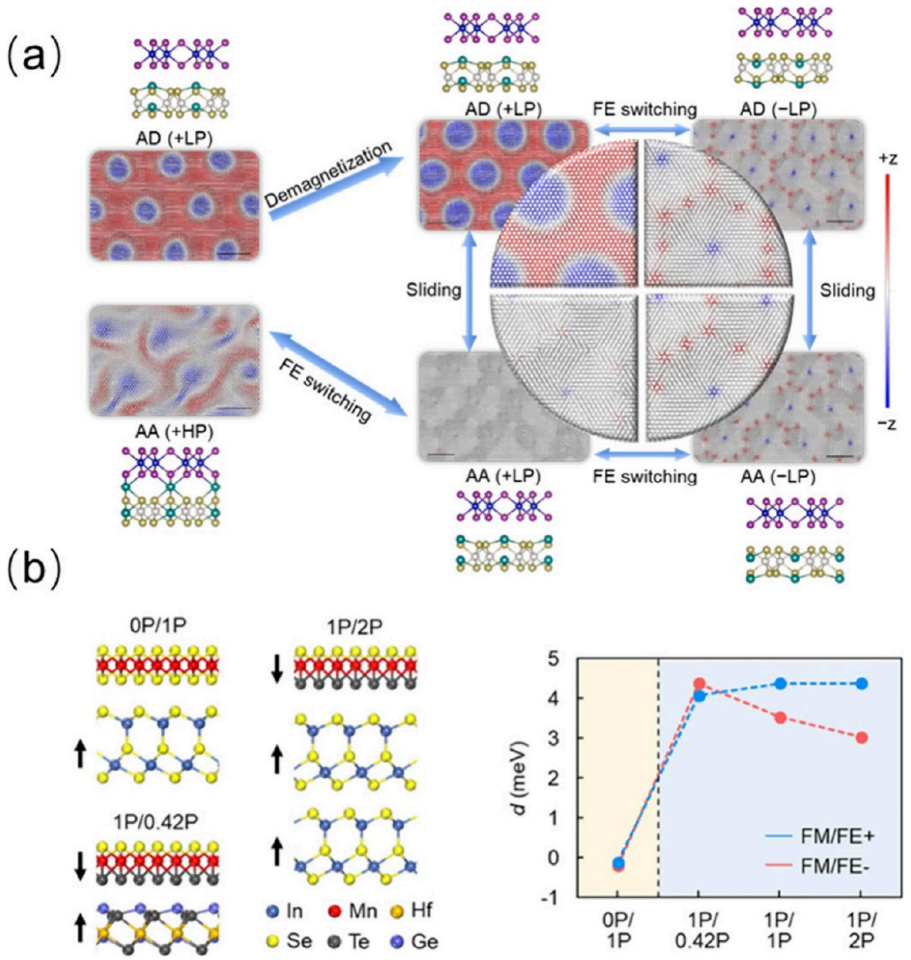

Figure 4. Ferroelectric modulation of topological spin textures and DMI. (a) Reversible magnetic configuration evolution for the $CrI_3/Pt_2Sn_2Te_6$ heterojunction as interlayer sliding and ferroelectric polarization switching.[7] Copyright 2024, American Chemical Society. The black scale bar corresponds to 10 nm. (b) The effects of polarization-polarization interaction on magnetoelectric coupling.[29] Copyright 2023, IOP Publishing. Atomic configurations of $MnSe_2/In_2Se_3$, $MnSeTe/Hf_2Ge_2Te_6$, and $MnSeTe/bilayer\text{-}In_2Se_3$ heterostructures, which are denoted as 0P/1P, 1P/0.42P, and 1P/2P, respectively. Here mP/nP represents the polarizations of FM and FE materials relative to $MnSeTe/In_2Se_3$ (1P/1P). FE+ and FE− represent upward and downward ferroelectric polarization, respectively.

configurations, magnetic skyrmions—topologically protected whirling spin textures—have garnered significant attention.[28] Their potential applications in next-generation information storage and processing devices, such as racetrack memory, logic computation, transistor-like functional devices, and neuromorphic systems, make them particularly promising. In various applications, there are common requirements for magnetic skyrmions, including precise, low-energy control over their creation and erasure, maintaining the directionality of skyrmion transport, and ensuring the stability of information storage. Magnetic proximity effects play a crucial role in these aspects.

The generation and stability of magnetic skyrmions depend on appropriate magnetic interactions within the magnetic material, while the erasure of magnetic skyrmions is directly related to the absence of stability conditions. The Hamiltonian of magnetic interactions can be expressed as

$$H = -J\sum_{\langle ij<>\rangle} \boldsymbol{S}_i \bullet \boldsymbol{S}_j - \sum_{\langle ij<>\rangle} \boldsymbol{D}_{ij} \bullet (\boldsymbol{S}_i \times \boldsymbol{S}_j) - K\sum_i (\boldsymbol{S}_i \bullet \hat{\boldsymbol{z}})^2 - \sum_i \mu_i \boldsymbol{B} \bullet \boldsymbol{S}_i + E_{\text{other}} \quad (6)$$

where the first to fourth terms are exchange interaction, DMI, MAE, and Zeeman energy, respectively. The last term includes higher-order exchange interactions. Despite various mechanisms to generate magnetic skyrmions, the manipulation of DMI plays a central role in stabilizing chiral spin textures in magnetic materials. DMI arises from SOC in systems without inversion symmetry. Interface-induced interfacial DMI can be attributed to the breaking of the inversion symmetry at the interface between two materials. The strong SOC mainly originates from heavy atoms at the interface, leading to a noncollinear spin arrangement, which results in the stabilization of chiral magnetic structures, such as skyrmions. The magnitude and direction of this interfacial DMI can be tuned by altering the properties of the substrate, the thickness of the magnetic film, the interfacial quality, the interlayer sliding, and the interlayer rotation. Consequently, it provides a versatile approach to controlling the size, stability, and dynamics of magnetic skyrmions for advanced spintronic applications.

Recently, Li et al. reported that by constructing multiferroic heterojunction using FM CrI_3 and quadruple-well FE $Pt_2Sn_2Te_6$, a nonvolatile multistate control of topological magnetism in the magnetic material can be achieved.[7] The $Pt_2Sn_2Te_6$ exhibits four ferroelectric polarization states, i.e.,

https://doi.org/10.1021/acs.nanolett.4c04251
Nano Lett. XXXX, XXX, XXX−XXX

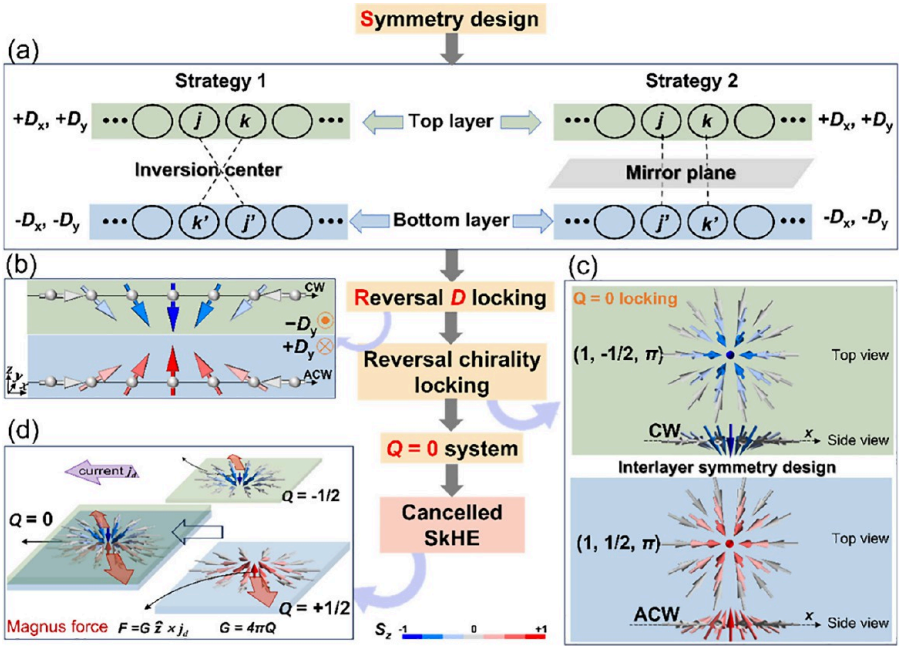

Figure 5. Interlayer interaction induced zero Q of topological spin textures in double-magnetic-atomic-layer ferromagnets.[30] Copyright 2024, American Chemical Society. (a) Schematics of designed systems containing two ferromagnetic layers connected by inversion symmetry or mirror symmetry. The j and k atoms in the top layer correspond to the j' and k' atoms in the bottom layer due to the inversion or mirror symmetry. (b) The relationship between the sign of D_y and the chirality along the x direction. ACW and CW represent the anticlockwise and clockwise chirality, respectively. (c) An example of $Q = 0$ locked interlayer Néel bimerons. (d) Schematics of the canceled skyrmion Hall effect of the system.

high polarization states along the z (+HP) and $-z$ direction (−HP), low polarization states along the z (+LP) and $-z$ direction (−LP), respectively. Figure 4 shows the evolution of magnetic spin textures of $CrI_3/Pt_2Sn_2Te_6$ in response to ferroelectric polarization switching and interlayer sliding. More details regarding the stacking modes can be found in the previous literature.[7] As shown in Figure 4a, starting from AD stacking and the + LP state of the $CrI_3/Pt_2Sn_2Te_6$ heterojunction, a regular Bloch-type skyrmion lattice is achieved by an external out-of-plane magnetic field ranging from 0.5 to 1.7 T. After demagnetization, the regular skyrmion lattice remains. The ferroelectric polarization switching to AD (−LP) states results in a new regular magnetic superstructure. After interlayer sliding and ferroelectric switching to another stacking mode, the magnetic spin textures can switch to in-plane magnetism. Each transform process among these spin textures is reversible.

In addition to the control of magnetic interactions by ferroelectric polarization and interlayer sliding, Jin et al. have also found that the polarization state of the magnetic material itself will affect the strength of the magnetoelectric coupling in ferroelectric-ferromagnetic heterojunctions, as well as the control of DMI by ferroelectric polarization.[29] Figure 4b shows the effects of the polarization-polarization (P−P) interaction on magnetoelectric coupling. In the case of the $MnSe_2/In_2Se_3$ heterostructure (0P/1P configuration) without P−P interactions, it is apparent that the magnetic parameters undergo minimal ferroelectric modulation (shifting from red to blue dots), suggesting weak magnetoelectric coupling. Nonetheless, upon intensifying the P−P interactions (ranging from 1P/0.42P to 1P/2P), there is a notable augmentation in the magnetoelectric coupling between the FM and ferroelectric constituents. Therefore, the P−P interaction emerges as a pivotal factor in enhancing the magnetoelectric coupling and tunability of magnetic interactions.

The Skyrmion Hall effect (SkHE) characterized by the transverse motion of magnetic skyrmions when subjected to a longitudinal current drive is another challenge during the application of skyrmion. SkHE leads to skyrmion pinning and even data loss in storage applications. To address this challenge, it is essential to eliminate SkHE. One of the most promising approaches to achieving this goal is the construction of topological structures with zero topological charge number (Q),[30] because the transverse motion velocity is proportion to Q.

Taking the ferromagnetic bilayer system as an example, Figure 5 describes the design strategy to achieve zero Q of topological spin texture in double-magnetic-atomic-layer ferromagnets.[30] The Q can also be expressed by $Q = m \bullet p$, where polarity $p = -\frac{1}{2}\cos\theta(r)|_{r=0}^{\infty}$ and vorticity $m = \frac{1}{2\pi}\Phi(\phi)\Big|_{\phi=0}^{2\pi}$.[28] If one of the polarity and vorticity of the topological spin texture in the two magnetic layers is the same while the other is opposite, a zero Q of the whole system can be achieved. Because the polarity and vorticity of Bloch, Néel type and antitype skyrmions are fixed by the spin orientation of FM background, the interlayer FM coupled biskyrmions cannot be a zero Q topological spin texture. However, the polarity of merons is not fixed by the FM background, offering the possibility to achieve a zero Q of interlayer coupled topological spin texture. To simplify the theoretical model, the authors focused on a system with inversion or in-plane mirror symmetry, as shown in Figure 5a. Both symmetries of the system would induce opposite in-plane DMI within the two magnetic layers. Because $H_{DMI} = \sum_{\langle ij<>\rangle} \boldsymbol{D}_{ij} \bullet (\boldsymbol{S}_i \times \boldsymbol{S}_j)$, opposite DMI induces opposite

https://doi.org/10.1021/acs.nanolett.4c04251
Nano Lett. XXXX, XXX, XXX−XXX

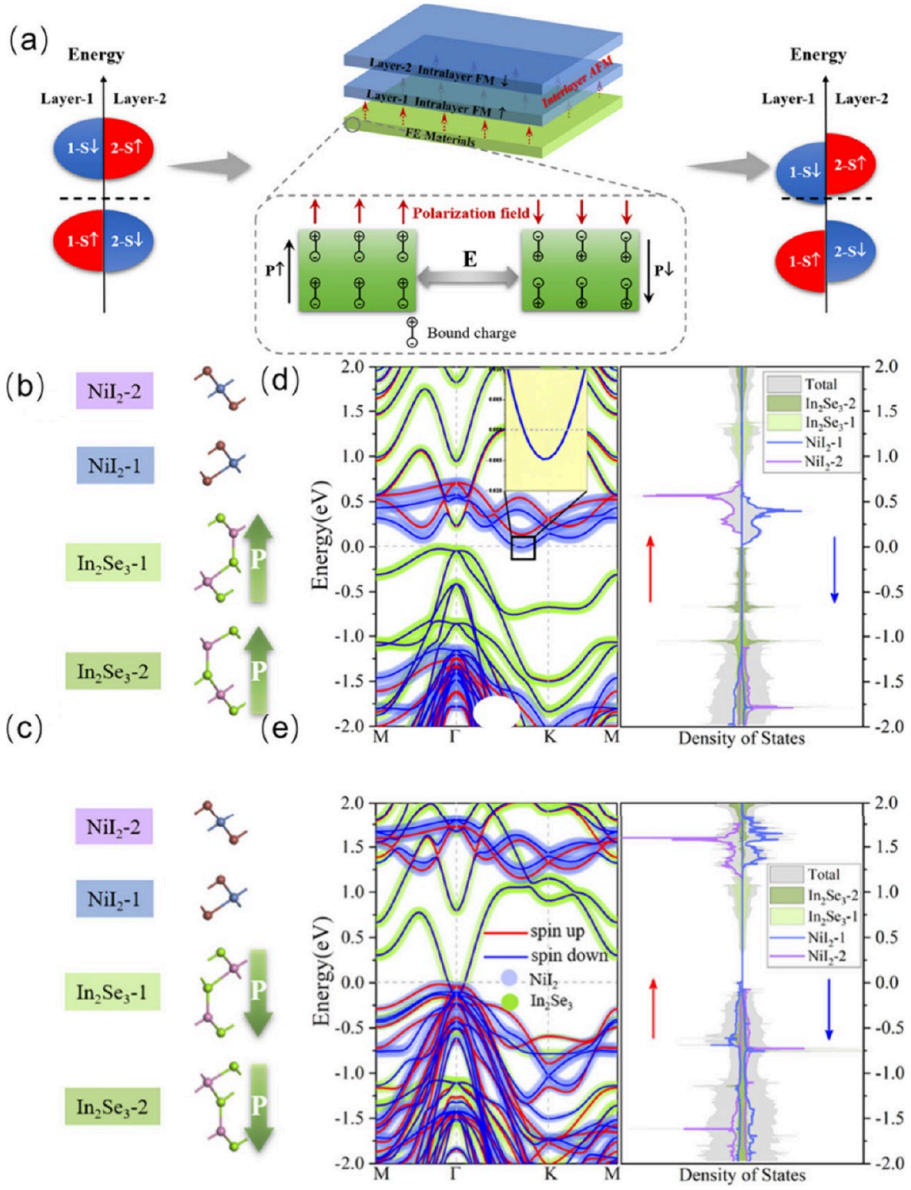

Figure 6. Ferroelectric control of half-metallicity of bi-NiI_2/bi-In_2Se_3 heterojunction.[34] Copyright 2022, Springer Nature. (a) Schematic illustration of ferroelectric polarization modulated spin-polarized density of states. Structures of bi-NiI_2/bi-In_2Se_3 heterojunctions with (b) up ferroelectric polarization P↑ and (c) down ferroelectric polarization P↓ configurations. Calculated band structures and density of states of bi-NiI_2/In_2Se_3 heterostructure with (d) P↑ and (e) P↓ configurations, respectively. The red and blue lines in the band structure represent spin-up and spin-down states, respectively.

chirality (Figure 5b). Figure 5c shows the case of interlayer coupled bimeron with opposite chirality, i.e., a clockwise (CW) chirality in the upper layer Meron and an anticlockwise (ACW) chirality in the lower layer Meron. Their polarities are opposite, and the total Q of the system is zero. The elimination of SkHE is thus achieved, as shown in Figure 5.

In addition to modulating magnetic interactions, the proximity effect can also profoundly influence the electronic structure through interlayer orbital hybridization. Strong interlayer interactions are crucial for regulating the electronic structure properties of magnetic 2D materials. The interaction enhancement can be achieved by selecting materials with specific characteristics. To illustrate this, the selection of materials with out-of-plane delocalized orbitals, such as black phosphorus (BP), can facilitate interlayer coupling. Among structurally similar materials, such as transition metal dichalcogenides, stronger interlayer interactions are typically observed when the central cation remains the same and the anion exhibits a lower electronegativity or a larger atomic mass.[31]

The integration of two-dimensional magnetic materials with 2D ferroelectric materials to create multiferroic heterostructures enables precise control of the electronic structure of the magnetic materials through the manipulation of the ferroelectric polarization directions. This approach is widely recognized for its efficiency and is a prevalent method of choice. The distinct polarization directions in the ferroelectric layers result in distinct interfacial interactions and electronic structures. This interfacial interaction allows for the precise control over the height of interfacial barriers,[32] spin polarization,[33] and the properties ranging from metallic to semiconducting to halfmetallic.

https://doi.org/10.1021/acs.nanolett.4c04251
Nano Lett. XXXX, XXX, XXX−XXX

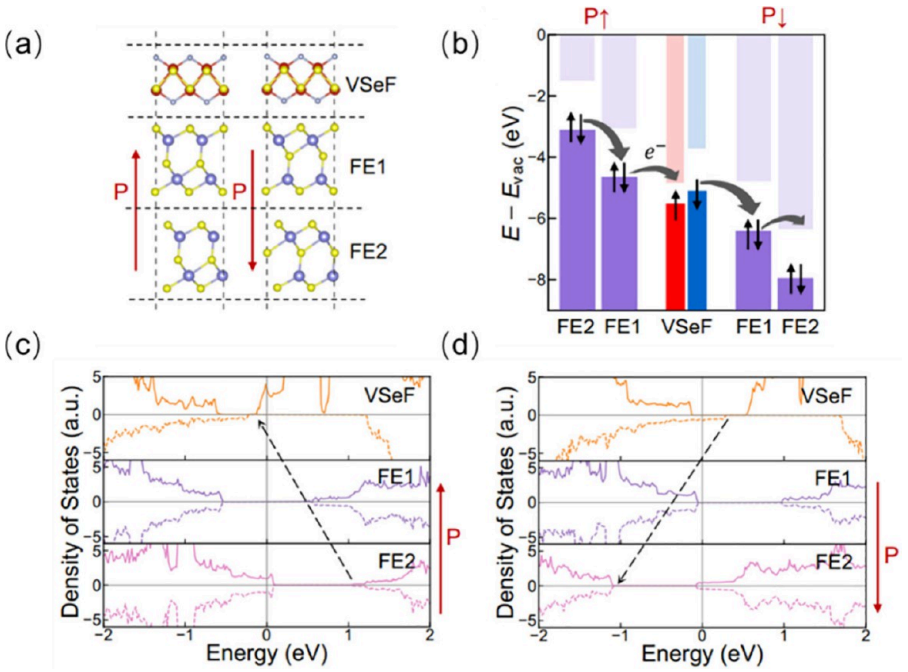

Figure 7. Ferroelectric control of spin polarization of VSeF/biAl$_2$Se$_3$ trilayer heterostructures.[36] Copyright 2023, Springer Nature. (a) Side views of VSeF/biAl$_2$Se$_3$ trilayer heterostructures. The red arrow represents the polarization direction of Al$_2$Se$_3$. (b) Band alignments of VSeF/biAl$_2$Se$_3$(↑) and VSeF/biAl$_2$Se$_3$(↓) with respect to the vacuum level of VSeF. The red and blue bars depict the band edges of spin-up and spin-down channel of VSeF, respectively. The purple bars depict the band edges of two layers of FE Al$_2$Se$_3$. (c) and (d) Layer-resolved PDOS of VSeF/biAl$_2$Se$_3$(↑) and VSeF/biAl$_2$Se$_3$(↓). The potential energy decreases along the direction of black dashed line. FE1 and FE2 denote the upper Al$_2$Se$_3$ layer and the bottom Al$_2$Se$_3$ layer, respectively. The orange, purple, and pink lines represent the PDOS contributed by VSeF, FE1, and FE2, respectively.

Figure 6a illustrates the design strategy to achieve reverse control of the transition from half-metallicity to semiconducting behavior, where bilayer magnetic materials with AFM interlayer coupling and FM intralayer coupling are coupled with a FE material.[34] The polarization field and potential interfacial charge transfer, resulting from the work function difference, are expected to generate an electrostatic potential difference between the two FM layers. The following example illustrates one possible case. The up ferroelectric polarization of the FE material leads to the downward shift of the DOS associated with layer-1 (the bottom FM layer) with respect to that of layer-2 (the top FM layer). Conversely, a down ferroelectric polarization of the FE material leads to the upward shift of the DOS associated with layer-1 with respect to that of layer-2. The final result is a switchable half-metallicity or magnetic semiconducting behavior for the heterojunction, depending on the position of the E_F energy. Figure 6b,d, and Figure 6c,e show the geometric structure and electronic structures of bilayer NiI$_2$ (bi-NiI$_2$) on bilayer In$_2$Se$_3$ (bi-In$_2$Se$_3$) with up and down ferroelectric polarization, respectively. Under an up ferroelectric polarization, the E_F passes through the spin-down conduction band edge, thereby exhibiting half-metallicity (see Figure 6d). The DOS analysis indicates that the electronic states at the E_F are contributed by the NiI$_2$-1 layer, while the NiI$_2$-2 layer retains the semiconducting property. By reversing the electric polarization of bi-In$_2$Se$_3$, the energy bands associated with the bi-NiI$_2$ shift upward relative to the E_F, and the intersection between them is eliminated, implying that the bi-NiI$_2$ restores the semiconducting nature, as depicted in Figure 6e. Figure 6 presents one strategy for controlling the spin polarization of an antiferromagnetically coupled bilayer through ferroelectric polarization and demonstrating the theoretical feasibility of this approach. It is important to note that in the structure model displayed, the magnetic order of monolayer and bilayer NiI$_2$ is simplified to the most basic collinear out-of-plane AFM configuration. However, the actual magnetic structure of monolayer and bilayer NiI$_2$ is more complex, and the understanding of them is still developing.[35]

Li et al. employed an alternative strategy to control the spin polarization in multiferroic heterojunctions,[36] specifically by incorporating an intrinsic bipolar magnetic semiconductor VSeF in conjunction with a ferroelectric bilayer of Al$_2$O$_3$, as shown in Figure 7a. In the monolayer VSeF, the conduction-band minimum (CBM) and valence-band maximum (VBM) of monolayer VSeF are derived from the spin-up and spin-down channels, respectively, as illustrated by the band alignment when integrated with the Al$_2$O$_3$ bilayer in Figure 7b. When the multiferroic trilayer system is in an upward ferroelectric polarization state, the VBM of the FE gate is positioned above the CBM of the VSeF, facilitating electron transfer from biAl$_2$O$_3$ to the VSeF. Consequently, an n-doped VSeF with spin-up carriers is formed within the system. In contrast, when the ferroelectric polarization of biAl$_2$O$_3$ is reversed, the VBM of VSeF surpasses the CBM of Al$_2$O$_3$, prompting an opposite electron transfer, which results in the appearance of a p-doped VSeF layer with spin-down carriers. Figure 7c,d demonstrates the projected density of states for the trilayer system under both ferroelectric polarization states, thereby confirming the nonvolatile electric manipulation of spin polarization within the system.

The quantum anomalous Hall effect (QAHE), characterized by quantized Hall conductance in the absence of an external magnetic field, is host to dissipationless chiral edge states. This characteristic renders QAHE an energy-efficient platform for state-of-the-art applications in spintronics and quantum

https://doi.org/10.1021/acs.nanolett.4c04251
Nano Lett. XXXX, XXX, XXX−XXX

computing.[37] To date, several strategies have been proposed for inducing the QAHE, including the use of magnetically doped topological insulators,[38] intrinsic magnetic topological insulators,[39] magnetic moiré materials,[40] and magnetic heterojunctions.[10,41,42] Among these, magnetic heterojunctions offer a multitude of combinations by pairing two distinct materials—either a magnet insulator with a topological insulator or two magnetic insulators. Despite some limitations, such as a weak proximity effect, this strategy is particularly advantageous, as it can potentially circumvent several challenges associated with QAHE, including disorder scattering caused by defects, the maintenance of stable magnetic ordering, and the limited availability of intrinsic magnetic topological insulators.

Figure 8 shows two design principles for constructing a topological magnetic heterojunction, either by integrating a topological insulator (TI) with a magnetic semiconductor or two magnetic semiconductors with type-III broken-gap alignment. For the first case (Figure 8a), the time reversal symmetry (TRS) of the TI is broken by the magnetic proximity effect, leading to band crossing at the Fermi energy. In the second case (Figure 8b), band cross occurs at the Fermi energy due to the type III broken gap band alignment. When the SOC is taken into account, the bulk band gap can be opened in both cases. Whether the SOC-induced insulating state is topologically nontrivial or not can be identified by calculating the Berry curvature and the Chern number.[43]

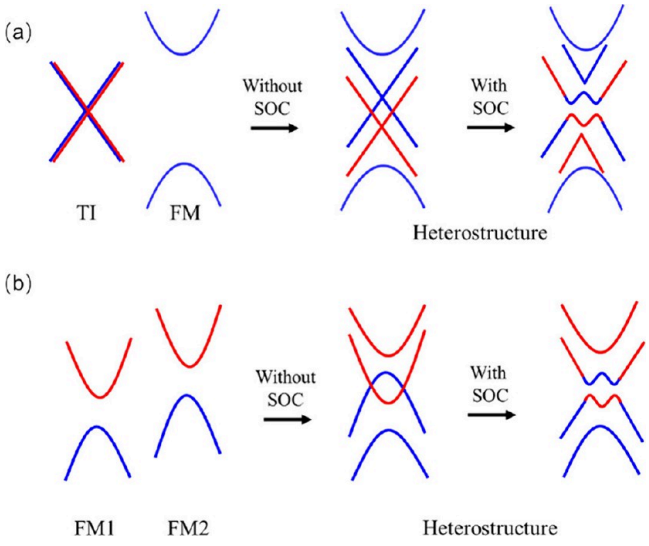

Figure 8. Two design principles of topological magnetic heterojunction. Band structure of magnetic heterojunction comprising (a) a combination of topological insulator and a magnetic semiconductor, and (b) two magnetic semiconductors with proper band alignment.

In 2020, Cui et al. theoretically reported a giant enhancement of perpendicular magnetic anisotropy and induced quantum anomalous Hall effect in graphene/NiI_2 heterostructures via tuning the vdW interlayer distance.[41] In their model, the magnetism of NiI_2 was also simplified as collinear ferromagnetism. They found that the NiI_2 substrate induces strong magnetic proximity effects on graphene and that the quantum anomalous Hall effect (QAHE) can be acquired by decreasing the interlayer spacing. Figure 9a shows the geometric structure of graphene/NiI_2 with a vertical distance d. For the heterojunction with an equilibrium interlayer distance (Δd = 0 Å), the band structure without considering SOC (Figure 9b) shows a metallic character. As shown in Figure 9c, a reduction in the interlayer distance results in movement of the Dirac cones within the band gap of NiI_2. The enhanced proximity effect induces an exchange splitting of about 87 meV in graphene (Figure 9d), which can be explained by a Rashba mechanism. When SOC is included, small band gaps open at the crossing point of two bands, and the E_F is right inside the SOC band gaps as shown in Figure 9e. The distinct sublattices A and B of graphene give rise to SOC-induced band gaps around high-symmetry points, namely the K point and K' point, which exhibit differences of 4.42 and 2.19 meV, respectively (Figure 9f,g). By integration of the Berry curvatures over the Brillouin zone, a Chern number of −2 was obtained, thereby confirming the QAHE in compressed graphene/NiI_2.

The magnetic proximity effect can also be employed to enhance the stability of the QAHE of magnetic topological materials. For example, experiments have observed the presence of gapless surface states in the layered AFM $MnBi_2Te_4$ film, indicating the absence of out-of-plane surface magnetism. Hu et al. proposed that the formation of $MnBi_2Te_4/CrI_3$ heterojunction could induce a strong exchange bias of about 40 meV, stemming from the hybridization between the Cr-e_g orbital tails and Te p orbitals.[44] The stabilized surface magnetism in the $MnBi_2Te_4/CrI_3$ heterojunction gives rise to the emergence of QAHE, providing a platform to realize an electrically tunable zero-field QAHE.

In addition to constructing magnetic insulator- (magnetic) topological insulator heterojunction, Pan et al. proposed another approach to achieve QAHE via engineering 2D magnetic vdW heterojunctions with proper band alignment and frontier orbitals.[10] For the magnetic heterojunction building blocks, they focused on a family of ternary 2D materials MXY (M = metal atoms, X = N, S, Se, Te, Y = F, Cl, Br, I) with a $p2mm$ plane group. To illustrate, the geometric structure of the heterojunction is shown in Figure 10a. The first step to screen promising combinations of two 2D monolayers is making sure they can form the so-called type-III broken-gap junction, in which the CBM of one 2D material is lower in energy than the VBM of the other compound at certain high-symmetry momentum, as shown in Figure 10b. Next, they perform a generic symmetry analysis of topological properties for the heterojunctions. That analysis is based on the relationship between topological invariant, the Chern number (CN) that characterizes the QAH effect, and the 2-fold rotation (C2) eigenvalues. According to their analysis, the CN for the heterojunction must be changed by an odd number when the magnetizations in two magnetic vdW compounds are switched from FM to AFM stacking order, suggesting that the QAH phase must exist for at least one magnetic stacking order.

Taking the MnNF/MnNCl heterojunction as an example, they directly calculated its topological invariant and chiral edge states. Figure 10c,d shows projected band structures of freestanding MnNF and MnNCl monolayers. Mn cations are confined in a quasi-octahedral bonding environment associated with a t_{2g}−e_g d state splitting. The CBM of MnNF or MnNCl is composed of Mn e_g states, whereas the VBM is derived from the interaction between occupied N p states and Mn t_{2g} states. This unique electronic structure feature endows the VBM and CBM of MXY compounds with different C2 rotational eigenvalues. For the heterojunction with FM stacking order, without spin orbit coupling (SOC), the crossing in the same

https://doi.org/10.1021/acs.nanolett.4c04251
Nano Lett. XXXX, XXX, XXX−XXX

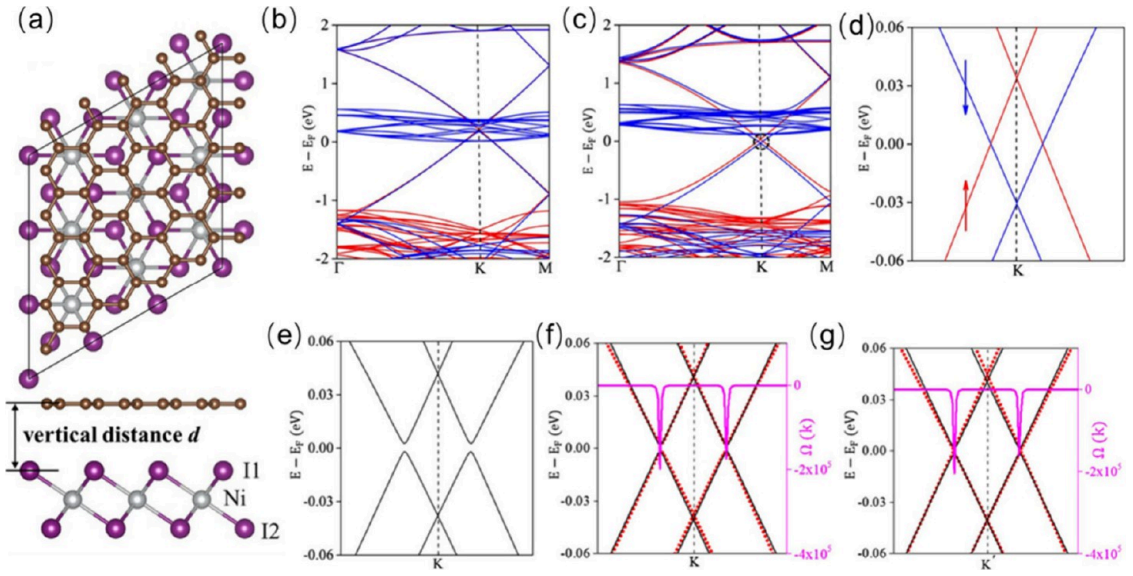

Figure 9. Magnetic proximity induced quantum anomalous Hall effect in graphene.[41] Copyright 2020, American Physical Society. (a) Top and side view of graphene/NiI_2 heterostructure. Purple, gray, and brown balls represent I, Ni, and C atoms, respectively. The band structure of (b) graphene/NiI_2 with Δd = 0 Å, and (c) Δd = −0.7 Å. (d) Zoom in on the black dashed circle of panel (c). Red and blue lines present the spin-up and spin-down bands, respectively. (e) The band structure of graphene/NiI_2 with Δd = −0.7 Å when SOC is considered. (f) The black lines and red dots represent the band structure obtained from the low-energy effective model and DFT calculations, respectively. The purple lines represent the calculated Berry curvature. (g) The same as (f), except around the K' point.

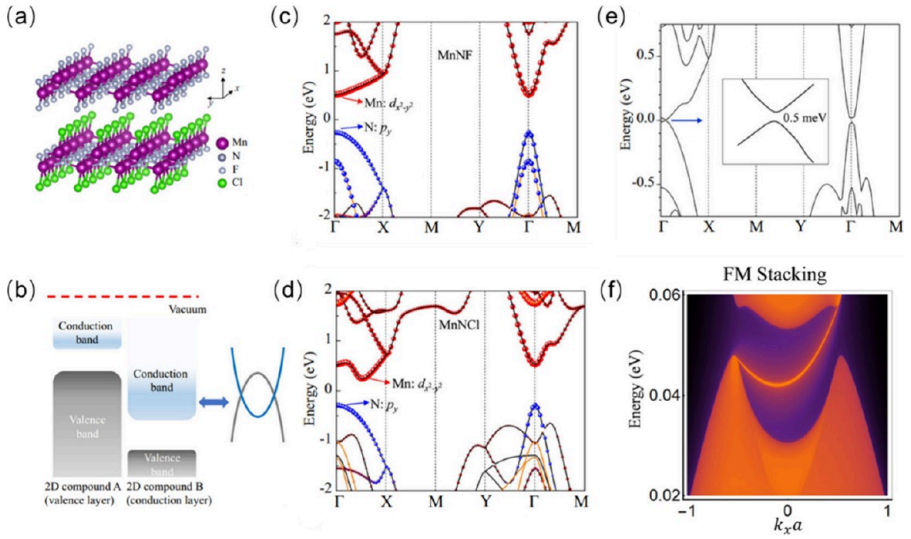

Figure 10. Band alignment induced quantum anomalous Hall effect in type-III broken-gap 2D magnetic heterojunction.[10] Copyright 2020, Springer Nature. (a) Geometric structure of MnNF/MnNCl heterojunction. (b) Schematic of type-III broken-gap 2D heterojunctions. (c, d) Band structure of freestanding MnNF and MnNCl, respectively. Black and orange curves represent spin up and spin down, respectively. Red dot and blue dot correspond to the $d_{x^2-y^2}$ orbitals of Mn and p_y orbital of N. (e, f) Band structures of MnNF/MnNCl heterojunction under FM stacking.

channel happens around the Γ point, leading to a 14.0 meV of band inversion, as shown in Figure 10e. The inclusion of SOC opens a band gap at the original crossing point located on the Γ-X line. However, the SOC is quenched by the crystal environment; the SOC gap is only around 0.5 meV. The authors claimed that sliding one layer along the y direction, introducing the mirror symmetry broken, can increase the gap to 6.0 meV. Using a tight-binding model, they further investigated the topological properties of the heterojunction. With reasonable parameter values, the band structure of FM stacked heterojunction are shown in Figure 10f, showing a chiral edge state connecting the CB and VB. The CN of the heterojunction in this case is 1, ensuring the emergence of quantum anomalous Hall effect.

Multiferroic materials, which exhibit two or more ferroic properties such as magnetism, ferroelectricity, ferroelasticity, and ferrovalley, hold immense potential for innovative regulatory mechanisms due to the interaction between their multiple order parameters.[45] For example, the coupling between ferroelectricity and magnetism enables the control of magnetic properties via electric fields and vice versa. This dual-control capability is not only crucial for understanding the complex relationship between electric and magnetic orders but also opens the door to a new generation of high-performance devices. The ability to control magnetic domains with electric

https://doi.org/10.1021/acs.nanolett.4c04251
Nano Lett. XXXX, XXX, XXX−XXX

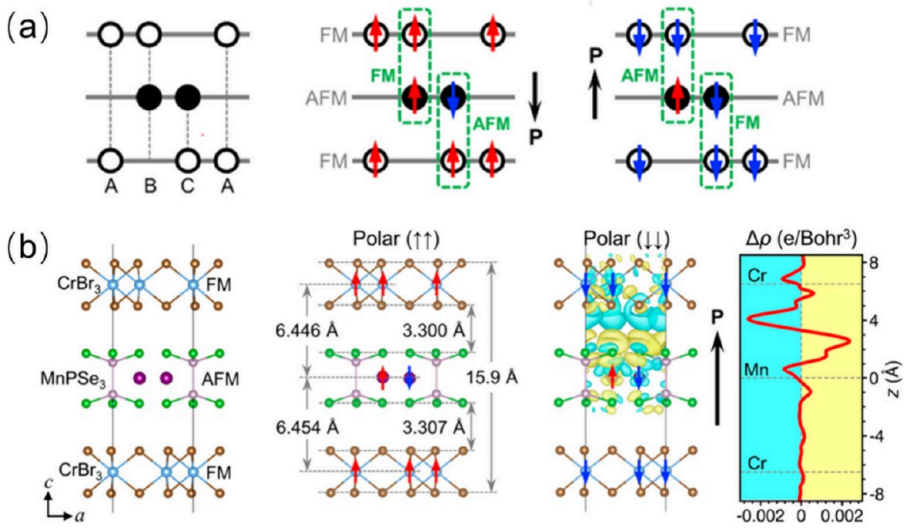

Figure 11. Spin-driven out-of-plane ferroelectric polarization in the ABC-stacked trilayer heterostructure.[47] Copyright 2023, American Chemical Society. (a) Design strategy for implementing the exchange striction spin structure in a 2D FM/AFM/FM sandwich system with ABC stacking configuration. Fixed the middle AFM layer, the opposite spin direction of the FM layers induces opposite ferroelectric polarization of the system. (b) Geometric structure, charge density difference, and integration of charge density difference of $CrBr_3/MnPSe_3/CrBr_3$ trilayer heterostructure with one spin configuration shown in Figure 10(a).

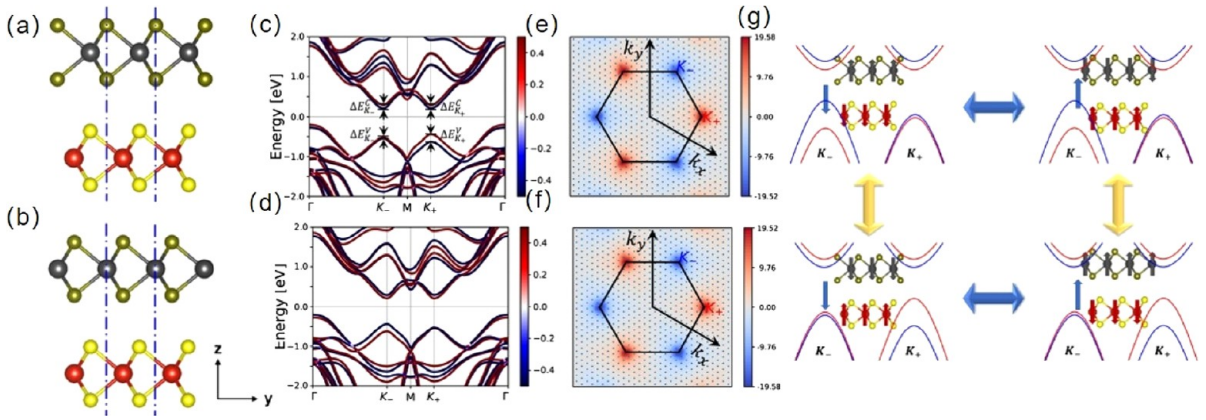

Figure 12. Stacking engineering of ferrovalley in 2D multiferroic bilayer VS_2.[48] Copyright 2020, American Physical Society. Panels (a) and (b) are the side views of the bilayer VS_2 structures in which the ferroelectric polarizations are along $-z$ and z axes, respectively. The band structure with SOC of ferroelectric AFM configurations P↓M↑↓ and P↑M↓↑ is shown in (c), and their Berry curvature distribution in the first Brillouin zone is shown in (e). The band structure with SOC of configurations P↓M↓↑ and P↑M↑↓ is shown in (d), and their Berry curvature is shown in (f). In (c) and (d), the red (blue) colors represent the bands of the spin projection in the positive (negative) directions of the z axis (spin up or spin down). (g) shows the multistates achievable in the multiferroic bilayer VS_2. The red and gray arrows represent the spin directions of the bottom layer and top layer VS_2, respectively. The blue arrows represent the ferroelectric polarization direction of the system. At the two energy valleys K_- and K_+, red and blue curves represent bands where the spin projection is positive (spin up) and negative (spin down) along the z axis, respectively.

fields, or to switch polarization with a magnetic field, can lead to energy-efficient and compact devices with improved integration potential in various electronic systems.[46] This makes them highly promising for developing multifunctional electronic devices, achieving energy-efficient, high-density data storage solutions, creating highly sensitive sensors, and advancing energy harvesting and conversion technologies. However, discovering high-performance multiferroic materials within a single substance is a significant challenge, given their distinct fundamental origins. By constructing 2D homojunctions or heterojunctions of magnetic materials, additional degrees of freedom for manipulation can be obtained, including not only ferroelectric polarization but also ferrovalley polarization and other emergent properties absent in their individual heterojunction building blocks. In 2023, Li et al. presented a theoretical design of a new class of 2D multiferroic systems.[7] These systems are vertically stacked vdW magnetic heterostructures that exhibit both ferromagnetism and ferroelectricity, which are properties that are usually challenging to control due to their distinct origins and symmetry constraints. The design strategy involves an FM chromium trihalide ($CrBr_3$) layer and an AFM $MnPSe_3$ layer. They demonstrate that by carefully designing the stacking order and magnetic configurations, it is possible to induce out-of-plane electric polarization in the heterostructure, which can be controlled by an external magnetic field. Figure 11a shows the mechanism of magnetic ordering induced ferroelectric polarization in the trilayer system with the ABC stacking mode. When imposing a magnetic structure that two FM layers are FM coupled, the inversion symmetry of the whole hetero-

https://doi.org/10.1021/acs.nanolett.4c04251
Nano Lett. XXXX, XXX, XXX−XXX

structure is broken, leading to the emergence of out-of-plane electric polarization via a similar mechanism in conventional type II multiferroics. Such electric polarization can be reversed by flipping the magnetization orientation of the two layers. Figure 11b verified such a design strategy by calculating the electric polarization of the $CrBr_3/MnPSe_3/CrBr_3$ trilayer heterostructure with one spin configuration shown in Figure 10a, demonstrating as expected up electric polarization of the whole system. The research offers a new route to control ferroelectricity through magnetic interactions in 2D materials.

Interlayer sliding within a magnetic homostructure emerges as another promising strategy for achieving the multiferroic property of 2D systems.[48] The ferroelectric polarization and ferrovalley polarization originate from the symmetry breaking of the system upon interlayer sliding of an in-plane translation. Utilizing first-principles density functional theory calculations, Liu et al. comprehensively studied the magnetoelectric properties of 2D multiferroic bilayer VS_2 and reported the coexistence of magnetism, ferroelectric polarization, and ferrovalley polarization within this system. The ground state of bilayer VS_2 is the 3R stacking structure as shown in Figure 12a or b. Each VS_2 layer has an FM state with an opposite magnetic moment between two AFM ordered layers. The out-of-plane ferroelectric polarization of bilayer VS_2 exists and can be reversed upon interlayer sliding. Accompanied by the transition of ferroelectric polarization, while keeping the magnetic ordering unchanged, the valley polarization changed, as shown in Figure 12c−g. That is, the extrema of the conduction band and valence band at the corners of the hexagonal Brillouin zones K_+ and K_- are different. Figure 12g shows the four possible states achievable in bilayer VS_2, which are degenerate in energy. However, how to control the transition among these states is still a big challenge.

In addition to the aforementioned properties, significant progress has been made in inducing and enhancing superconductivity and optical phenomena and performance through the construction of magnetic 2D material heterojunctions. For instance, researchers have discovered zero-energy bound states and enhanced superconducting gaps in the $MnTe/Bi_2Te_3/Fe(Te,Se)$ heterojunction.[49] Theoretical calculations have revealed that at the $MnTe/Bi_2Te_3$ interface, the spatial inversion is broken and there is strong SOC, resulting in a significant enhancement of the DMI between magnetic moments, a primary factor in the emergence of noncollinear magnetic structures, providing crucial signs for the generation of topological superconductivity. This offers a platform for realizing new types of topological superconductivity at magnetic/superconducting interfaces.

In bilayer CrI_3, researchers have found a nonreciprocal second-order nonlinear optical effect.[50] The observed second-harmonic generation is several orders of magnitude greater than known magnetization-induced SHG and is comparable to the SHG of the best-studied 2D nonlinear optical materials thus far (for example, molybdenum disulfide). The study indicates that this nonlinear optical coefficient originates from the interlayer AFM order, which breaks spatial inversion symmetry and time-reversal symmetry. This phenomenon opens up possibilities for the application of 2D magnets in nonlinear and nonreciprocal optical devices.

4. SUMMARY AND PERSPECTIVE

From a theoretical aspect, this paper reviews the fundamental physics of interlayer interaction and the enhancement and emergent properties of 2D magnetic heterojunction. It begins by introducing the fundamental physical properties of 2D magnetic materials, such as magnetic exchange interactions, DMI, and MAE. These interactions are essential for understanding the magnetic behavior of these materials. By regulation of interlayer orbital hybridization and breaking symmetry, intrinsic properties can be enhanced, new properties can be generated, and different properties can be reversibly controlled.

Regarding performance enhancement and emerging properties, the paper discusses engineering the proximity effect to manipulate the magnetism of 2D materials. For instance, by controlling the interlayer magnetic coupling through vdW gaps, an FM-AFM transition can be achieved. Research on Fe_4GeTe_2 demonstrates that reducing the number of layers can significantly increase T_c, highlighting the crucial role of interface modulation in the magnetism of 2D materials. The paper also discusses the generation and stability of magnetic skyrmions, topologically protected spin textures with potential applications in next-generation information storage and processing devices. By adjustment of the interfacial DMI, the size, stability, and dynamics of skyrmions can be effectively controlled. Additionally, the paper introduces the quantum anomalous Hall effect (QAHE) achieved through engineered 2D magnetic materials. QAHE, characterized by quantized Hall conductance without an external magnetic field, holds significant potential for spintronics and quantum computing applications. Finally, the paper discusses the multistate control of 2D magnetic heterostructures, presenting new strategies to achieve multiferroic properties by adjusting interlayer sliding. These studies offer new perspectives for understanding the fundamental physics of 2D magnetic materials and open new avenues for developing novel multifunctional electronic devices.

In the aforementioned theoretical proposals, approaches for tuning material properties include stacking layered materials with distinct electronic structures, inducing interlayer sliding, applying vertical stress, and reversing ferroelectric polarization. These approaches have been successfully demonstrated in other material systems, suggesting that experimental validation is, in principle, achievable. However, precise manipulation of interlayer sliding and vertical stress in heterostructures, along with the accurate detection of subtle atomic structural changes, presents significant challenges that require focused research efforts from experimental physicists.

Despite the theoretical calculations demonstrating the advantages and extraordinary potential of 2D magnetic heterostructures, there remains a significant gap between these materials and their practical application in electronic devices. Several challenges need to be addressed, including but not limited to the following areas:

First, the structural stability of materials poses a significant issue. Many theoretically predicted materials are obtained by substituting elements into certain prototype structures. However, many of these materials are thermodynamically and thermally unstable at room temperature, which limits their experimental preparation and characterization.

Second, the performance stability of the materials and structures is also a challenge. For the applications of magnetic materials, a T_c above room temperature is needed. Currently, only a few 2D magnetic metals meet this requirement. Additionally, achieving reversible control and characterization of properties of 2D magnetic heterojunctions in experiments is

https://doi.org/10.1021/acs.nanolett.4c04251
Nano Lett. XXXX, XXX, XXX−XXX

still challenging. For example, magnetic skyrmions are highly sensitive to interfacial interactions and may become unstable when considering substrates. To realize the quantum anomalous Hall effect, magnetic material heterostructures need to open a sufficiently large SOC gap near the Fermi level. However, in the currently predicted systems, the weak vdW interactions between layers can open a gap of only a few meV. In ferroelectric-ferromagnetic heterostructures, the ferroelectric polarization strength and switching barrier need to allow for reversible control by an electric field, but current theoretical calculations have paid little attention to this aspect. When valley polarization and magnetoelectric coupling of multiferroic properties through interlayer sliding are achieved, the weak vdW forces between layers may not provide sufficient transition barriers to stabilize the desired phase structures.

Furthermore, there are numerous control methods, such as twisted angle stacking homostructure, different dimensional stacking, and multilayer stacking, which introduce new physics and effects. However, due to computational and physical complexity, these aspects are still less explored.

Last but not least, although the interface control of magnetism holds great promise for future device applications, practical implementation requires a thorough understanding of electronic and thermal transport properties, and so on. The correlation between material properties and device performance has yet to be fully explored, which presents a critical challenge for future research. Developing more sophisticated models to predict device performance based on these heterojunctions and to establish clear correlations between material characteristics and device functionality is essential in the future.

AUTHOR INFORMATION

Corresponding Author

Shixuan Du − *Beijing National Laboratory for Condensed Matter Physics, Institute of Physics, Chinese Academy of Sciences, Beijing 100190, China; University of Chinese Academy of Sciences, Beijing 100049, China; Songshan Lake Materials Laboratory, Dongguan, Guangdong 523808, China;* orcid.org/0000-0001-9323-1307; Email: sxdu@iphy.ac.cn

Authors

Jinbo Pan − *Beijing National Laboratory for Condensed Matter Physics, Institute of Physics, Chinese Academy of Sciences, Beijing 100190, China; University of Chinese Academy of Sciences, Beijing 100049, China*

Yan-Fang Zhang − *University of Chinese Academy of Sciences, Beijing 100049, China*

Yu-Yang Zhang − *University of Chinese Academy of Sciences, Beijing 100049, China;* orcid.org/0000-0002-9548-0021

Complete contact information is available at: https://pubs.acs.org/10.1021/acs.nanolett.4c04251

Notes

The authors declare no competing financial interest.

ACKNOWLEDGMENTS

We acknowledge the financial support from the National Key Research and Development Program of China (2022YFA1204100, 2021YFA1201501), the National Natural Science Foundation of China (62488201, 52272172), and the Major Program of National Natural Science Foundation of China (92163206).

REFERENCES

(1) Mermin, N. D.; Wagner, H. Absence of ferromagnetism or antiferromagnetism in one-or two-dimensional isotropic Heisenberg models. *Phys. Rev. Lett.* **1966**, *17* (22), 1133.

(2) Huang, B.; Clark, G.; Navarro-Moratalla, E.; Klein, D. R.; Cheng, R.; Seyler, K. L.; Zhong, D.; Schmidgall, E.; McGuire, M. A.; Cobden, D. H.; Yao, W.; Xiao, D.; Jarillo-Herrero, P.; Xu, X. Layer-dependent ferromagnetism in a van der Waals crystal down to the monolayer limit. *Nature* **2017**, *546* (7657), 270−273.

(3) Gong, C.; Li, L.; Li, Z.; Ji, H.; Stern, A.; Xia, Y.; Cao, T.; Bao, W.; Wang, C.; Wang, Y.; Qiu, Z. Q.; Cava, R. J.; Louie, S. G.; Xia, J.; Zhang, X. Discovery of intrinsic ferromagnetism in two-dimensional van der Waals crystals. *Nature* **2017**, *546* (7657), 265−269.

(4) Choi, E. M.; Sim, K. I.; Burch, K. S.; Lee, Y. H. Emergent multifunctional magnetic proximity in van der Waals layered heterostructures. *Adv. Sci.* **2022**, *9* (21), 2200186.

(5) Li, D.; Li, S.; Zhong, C.; He, J. Tuning magnetism at the two-dimensional limit: a theoretical perspective. *Nanoscale* **2021**, *13* (47), 19812−19827.

(6) Wang, H.; Lu, H.; Guo, Z.; Li, A.; Wu, P.; Li, J.; Xie, W.; Sun, Z.; Li, P.; Damas, H.; Friedel, A. M.; Migot, S.; Ghanbaja, J.; Moreau, L.; Fagot-Revurat, Y.; Petit-Watelot, S.; Hauet, T.; Robertson, J.; Mangin, S.; Zhao, W.; Nie, T. Interfacial engineering of ferromagnetism in wafer-scale van der Waals Fe_4GeTe_2 far above room temperature. *Nat. Commun.* **2023**, *14* (1), 2483.

(7) Li, P.; Tao, L.; Jin, X.; Wan, G.; Zhang, J.; Zhang, Y. F.; Sun, J. T.; Pan, J.; Du, S. Nonvolatile multistate manipulation of topological magnetism in monolayer CrI_3 through quadruple-well ferroelectric materials. *Nano Lett.* **2024**, *24* (7), 2345−2351.

(8) Min, K.-H.; Lee, D. H.; Choi, S.-J.; Lee, I.-H.; Seo, J.; Kim, D. W.; Ko, K.-T.; Watanabe, K.; Taniguchi, T.; Ha, D. H.; Kim, C.; Shim, J. H.; Eom, J.; Kim, J. S.; Jung, S. Tunable spin injection and detection across a van der Waals interface. *Nat. Mater.* **2022**, *21* (10), 1144−1149.

(9) Deng, J.; Pan, J.; Zhang, Y.; Li, Y.; Dong, W.; Sun, J.; Du, S. Screening and design of bipolar magnetic-semiconducting monolayers and heterostructures. *ACS Appl. Electron. Mater.* **2022**, *4* (7), 3232−3239.

(10) Pan, J.; Yu, J.; Zhang, Y.-F.; Du, S.; Janotti, A.; Liu, C.-X.; Yan, Q. Quantum anomalous Hall effect in two-dimensional magnetic insulator heterojunctions. *NPJ. Comput. Mater.* **2020**, *6* (1), 152.

(11) Su, Y.; Li, X.; Zhu, M.; Zhang, J.; You, L.; Tsymbal, E. Y. Van der Waals multiferroic tunnel junctions. *Nano Lett.* **2021**, *21* (1), 175−181.

(12) Nie, J.-H.; Xie, T.; Chen, G.; Zhang, W.; Fu, Y.-S. Moiré enhanced two-band superconductivity in a $MnTe/NbSe_2$ heterojunction. *Nano Lett.* **2023**, *23* (17), 8370−8377.

(13) Cai, M.; Hao, Q.; Liu, J.; Dai, H.; Wang, X.; Chen, X.; Wang, H.; Xing, Y.; Chen, H.; Zhang, A.; Zhai, T.; Han, J. Topological magneto-optical effect from skyrmions in two-dimensional ferromagnets. *ACS Nano* **2024**, *18* (31), 20055.

(14) Huo, N.; Huang, L.; Shu, K.; Yang, M.; Luo, D.; Li, J. Improved photoluminescence in 2D semiconductors induced by interface magnetization. *ACS Photonics* **2020**, *7* (12), 3341−3345.

(15) Onga, M.; Sugita, Y.; Ideue, T.; Nakagawa, Y.; Suzuki, R.; Motome, Y.; Iwasa, Y. Antiferromagnet−semiconductor van der Waals heterostructures: Interlayer interplay of exciton with magnetic ordering. *Nano Lett.* **2020**, *20* (6), 4625−4630.

(16) Jiang, J.; Mi, W. Two-dimensional magnetic Janus monolayers and their van der Waals heterostructures: a review on recent progress. *Mater. Horiz.* **2023**, *10* (3), 788−807.

(17) Xiang, H.; Lee, C.; Koo, H. J.; Gong, X.; Whangbo, M. H. Magnetic properties and energy-mapping analysis. *Dalton Trans.* **2013**, *42* (4), 823−53.

(18) Hay, P. J.; Thibeault, J. C.; Hoffmann, R. Orbital interactions in metal dimer complexes. *J. Am. Chem. Soc.* **1975**, *97* (17), 4884−4899.

https://doi.org/10.1021/acs.nanolett.4c04251
Nano Lett. XXXX, XXX, XXX−XXX

(19) Liu, Y.-Z.; Zang, J. Overview and outlook of magnetic skyrmions. *Acta Phys. Sin-ch Ed.* **2018**, *67* (13), 131201.
(20) Gong, C.; Kim, E. M.; Wang, Y.; Lee, G.; Zhang, X. Multiferroicity in atomic van der Waals heterostructures. *Nat. Commun.* **2019**, *10* (1), 2657.
(21) Qiu, X.; Ji, W. Illuminating interlayer interactions. *Nat. Mater.* **2018**, *17* (3), 211−213.
(22) Moriya, T. Anisotropic superexchange interaction and weak ferromagnetism. *Phys. Rev.* **1960**, *120* (1), 91.
(23) Sivadas, N.; Okamoto, S.; Xu, X.; Fennie, C. J.; Xiao, D. Stacking-dependent magnetism in bilayer CrI_3. *Nano Lett.* **2018**, *18* (12), 7658−7664.
(24) Wang, C.; Zhou, X.; Zhou, L.; Pan, Y.; Lu, Z.-Y.; Wan, X.; Wang, X.; Ji, W. Bethe-Slater-curve-like behavior and interlayer spin-exchange coupling mechanisms in two-dimensional magnetic bilayers. *Phys. Rev. B* **2020**, *102* (2), 020402.
(25) Zhang, G.; Guo, F.; Wu, H.; Wen, X.; Yang, L.; Jin, W.; Zhang, W.; Chang, H. Above-room-temperature strong intrinsic ferromagnetism in 2D van der Waals Fe_3GaTe_2 with large perpendicular magnetic anisotropy. *Nat. Commun.* **2022**, *13* (1), 5067.
(26) Ruderman, M. A.; Kittel, C. Indirect exchange coupling of nuclear magnetic moments by conduction electrons. *Phys. Rev.* **1954**, *96* (1), 99.
(27) Anderson, P. W. Localized magnetic states in metals. *Phys. Rev.* **1961**, *124* (1), 41.
(28) Göbel, B.; Mertig, I.; Tretiakov, O. A. Beyond skyrmions: Review and perspectives of alternative magnetic quasiparticles. *Phys. Rep.* **2021**, *895*, 1−28.
(29) Jin, X.; O'Hara, A.; Zhang, Y.-Y.; Du, S.; Pantelides, S. T. Designing strong and tunable magnetoelectric coupling in 2D trilayer heterostructures. *2D Mater.* **2023**, *10* (1), 015007.
(30) Zhang, X.; Wan, G.; Zhang, J.; Zhang, Y.; Pan, J.; Du, S. Eliminating skyrmion Hall effect in ferromagnetic skyrmions. *Nano Lett.* **2024**, *24*, 10796.
(31) Mounet, N.; Gibertini, M.; Schwaller, P.; Campi, D.; Merkys, A.; Marrazzo, A.; Sohier, T.; Castelli, I. E.; Cepellotti, A.; Pizzi, G.; Marzari, N. Two-dimensional materials from high-throughput computational exfoliation of experimentally known compounds. *Nat. Nanotechnol.* **2018**, *13* (3), 246−252.
(32) Javaid, M.; Taylor, P. D.; Tawfik, S. A.; Spencer, M. J. Tuning the Schottky barrier height in a multiferroic In_2Se_3/Fe_3GeTe_2 van der Waals heterojunction. *Nanoscale* **2022**, *14* (11), 4114−4122.
(33) Zhang, X.; Zhou, Z.; Yu, X.; Guo, Y.; Chen, Y.; Wang, J. Ferroelectric control of polarity of the spin-polarized current in van der Waals multiferroic heterostructures. *Adv. Funct. Mater.* **2023**, *33* (32), 2301353.
(34) Wang, Y.; Xu, X.; Zhao, X.; Ji, W.; Cao, Q.; Li, S.; Li, Y. Switchable half-metallicity in A-type antiferromagnetic NiI_2 bilayer coupled with ferroelectric In_2Se_3. *NPJ. Comput. Mater.* **2022**, *8* (1), 218.
(35) Liu, N.; Wang, C.; Yan, C.; Xu, C.; Hu, J.; Zhang, Y.; Ji, W. Competing Multiferroic Phases in NiI_2 Mono-and Few-layers. *Phys. Rev. B* **2024**, *109*, 195422.
(36) Li, Y.; Deng, J.; Zhang, Y.-F.; Jin, X.; Dong, W.-H.; Sun, J.-T.; Pan, J.; Du, S. Nonvolatile electrical control of spin polarization in the 2D bipolar magnetic semiconductor VSeF. *NPJ. Comput. Mater.* **2023**, *9*, 50.
(37) Chang, C.-Z.; Liu, C.-X.; MacDonald, A. H. Colloquium: Quantum anomalous Hall effect. *Rev. Mod. Phys.* **2023**, *95* (1), 011002.
(38) Chang, C.-Z.; Zhang, J.; Feng, X.; Shen, J.; Zhang, Z.; Guo, M.; Li, K.; Ou, Y.; Wei, P.; Wang, L.-L. Experimental observation of the quantum anomalous Hall effect in a magnetic topological insulator. *Science* **2013**, *340* (6129), 167−170.
(39) Deng, Y.; Yu, Y.; Shi, M. Z.; Guo, Z.; Xu, Z.; Wang, J.; Chen, X. H.; Zhang, Y. Quantum anomalous Hall effect in intrinsic magnetic topological insulator $MnBi_2Te_4$. *Science* **2020**, *367* (6480), 895−900.
(40) Tseng, C.-C.; Ma, X.; Liu, Z.; Watanabe, K.; Taniguchi, T.; Chu, J.-H.; Yankowitz, M. Anomalous Hall effect at half filling in twisted bilayer graphene. *Nat. Phys.* **2022**, *18* (9), 1038−1042.
(41) Cui, Q.; Liang, J.; Yang, B.; Wang, Z.; Li, P.; Cui, P.; Yang, H. Giant enhancement of perpendicular magnetic anisotropy and induced quantum anomalous Hall effect in graphene/NiI_2 heterostructures via tuning the van der Waals interlayer distance. *Phys. Rev. B* **2020**, *101* (21), 214439.
(42) Zhang, H.; Qin, W.; Chen, M.; Cui, P.; Zhang, Z.; Xu, X. Converting a two-dimensional ferromagnetic insulator into a high-temperature quantum anomalous Hall system by means of an appropriate surface modification. *Phys. Rev. B* **2019**, *99* (16), 165410.
(43) Yao, Y.; Kleinman, L.; MacDonald, A. H.; Sinova, J.; Jungwirth, T.; Wang, D.-s.; Wang, E.; Niu, Q. First Principles Calculation of Anomalous Hall Conductivity in Ferromagnetic bcc Fe. *Phys. Rev. Lett.* **2004**, *92* (3), 037204.
(44) Hu, C.; Ding, L.; Gordon, K. N.; Ghosh, B.; Tien, H.-J.; Li, H.; Linn, A. G.; Lien, S.-W.; Huang, C.-Y.; Mackey, S. Realization of an intrinsic ferromagnetic topological state in $MnBi_8Te_{13}$. *Sci. Adv.* **2020**, *6* (30), No. eaba4275.
(45) Xun, W.; Wu, C.; Sun, H.; Zhang, W.; Wu, Y.-Z.; Li, P. Coexisting magnetism, ferroelectric, and ferrovalley multiferroic in stacking-dependent two-dimensional materials. *Nano Lett.* **2024**, *24* (11), 3541−3547.
(46) Zhang, J. J.; Lin, L.; Zhang, Y.; Wu, M.; Yakobson, B. I.; Dong, S. Type-II multiferroic $Hf_2VC_2F_2$ MXene monolayer with high transition temperature. *J. Am. Chem. Soc.* **2018**, *140* (30), 9768−9773.
(47) Li, H.; Zhu, W. Spin-driven ferroelectricity in two-dimensional magnetic heterostructures. *Nano Lett.* **2023**, *23* (22), 10651−10656.
(48) Liu, X.; Pyatakov, A. P.; Ren, W. Magnetoelectric coupling in multiferroic bilayer VS_2. *Phys. Rev. Lett.* **2020**, *125* (24), 247601.
(49) Ding, S.; Chen, C.; Cao, Z.; Wang, D.; Pan, Y.; Tao, R.; Zhao, D.; Hu, Y.; Jiang, T.; Yan, Y.; Shi, Z.; Wan, X.; Feng, D.; Zhang, T. Observation of robust zero-energy state and enhanced superconducting gap in a trilayer heterostructure of $MnTe/Bi_2Te_3/Fe(Te, Se)$. *Sci. Adv.* **2022**, *8* (37), No. eabq4578.
(50) Sun, Z.; Yi, Y.; Song, T.; Clark, G.; Huang, B.; Shan, Y.; Wu, S.; Huang, D.; Gao, C.; Chen, Z.; McGuire, M.; Cao, T.; Xiao, D.; Liu, W.-T.; Yao, W.; Xu, X.; Wu, S. Giant nonreciprocal second-harmonic generation from antiferromagnetic bilayer CrI_3. *Nature* **2019**, *572* (7770), 497−501.

https://doi.org/10.1021/acs.nanolett.4c04251
Nano Lett. XXXX, XXX, XXX−XXX